EVS27
Barcelona, Spain, November 17-20, 2013

Towards advanced BMS algorithms development for (P)HEV and EV by use of a physics-based model of Li-ion battery systems

E. Prada[1,2], D. Di Domenico[1], Y. Creff[1], V. Sauvant-Moynot[1]

[1]*IFP Énergies Nouvelles, Rond-point de l'échangeur de Solaize,BP3 69360 Solaize, France*
[2]*Corresponding author : eric.prada@ifpen.fr*

Abstract

Onboard Hybrid Electric Vehicles (HEV) and Battery Electric Vehicles (BEV), the Battery Management System (BMS) is of critical importance to ensure safe and reliable use of the electrical energy stored inside Li-ion batteries until the End-Of-Life (EOL) of the electrochemical system. At any time, the BMS must indicate the allowable current limits for charge and discharge (CMI: Charge Maximal Intensity and DMI: Discharge Maximal Intensity) that the battery systems can safely absorb/supply at different temperatures (T) and states-of-charge (SOC) for a given pulse duration (t_{pulse}) according to the electric power absorbed by the vehicle operational usage. CMI and DMI laws are generally specified by the battery manufacturer based on experimental tests campaigns. In this paper, BMS specifications laws are investigated for $Li(Ni_xCo_yAl_z)O_2$/Graphite (NCA/C) Li-ion technology through a physics-based battery model which allows the analysis of different physical phenomena that impact the system performance according to operating conditions. The CMI and DMI are then compared to the battery manufacturer data. Finally, the DMI and CMI are implemented in a Battery Intensity Management Algorithm (BIMA) which is validated at the simulation level. This practical method can be generalized to other Li-ion chemistries, enabling efficient model-based design of conventional BMS laws with regard to cell limits in terms of (over)potentials, current, temperature, and aging mechanisms.

Keywords: Li-ion electrochemical and thermal modeling, Battery management systems laws, Maximum charge and discharge current intensities

1   Introduction

During the past decade, Li-ion batteries have become the most promising candidates for Hybrid Electric Vehicles (HEV) and Battery Electric Vehicles (BEV) due to their high specific power and energy. However, these batteries technologies have to be carefully managed to prevent from possible safety issues such as fire or explosion. The Battery Management System (BMS) has to ensure a safe and reliable use of the electrical energy stored onboard HEV and BEV. Among all the conventional BMS functions such as state-of-charge (SOC) estimation, cell balancing, overcharge/discharge protection, a key information is to know the current intensity, *I*, that can be provided to/extracted from the battery system at any time. Different approaches can be found to

estimate/specify the values of current intensity that can be used during the battery operation. The Charge Maximal Intensity (CMI) and Discharge Maximal Intensity (DMI) can be either determined by experimental procedures and are generally provided by the battery cell manufacturer [1,2], or calculated by a model-based algorithm that can estimate the available charge or discharge power/current intensity [3,4,5]. In this paper, an analysis of the CMI and DMI through a physics-based model is performed for HEV/BEV applications. A way to understand and streamline costly experimental characterization procedures by means of a reduced order multi-physics based model is proposed. In section 2, the generic electrochemical-thermal coupled Li-ion battery model is presented and experimentally validated for a Li(Ni$_x$Co$_y$Al$_z$)O$_2$/Graphite (NCA/C) technology (VL41M from SAFT [6]). In section 3, the CMI and DMI of the selected battery are designed, analysed and discussed with regards to cell limit specifications from the manufacturer. In section 4, the model-based BMS laws design methodology is used within a battery intensity monitoring algorithm (BIMA) for (P)HEV/EV applications that could be implemented in a BMS. Different numerical case studies are proposed to validate the designed BIMA. In conclusion, the capabilities and limits of the approach are discussed as well.

2 Electrochemical and Thermal Li-ion Battery Model

During the past two decades, increasing research and development efforts have been performed to understand and model the complex Li-ion battery behaviours and performance all over the system lifetime. Different modeling approaches can be found in the literature, from simple electric equivalent circuit models [7] to complex Pseudo-2-Dimensional electrochemical and thermal models [4]. Recently, many groups have been working on the development of reduced order models (ROM) that combine the computing efficiency of empirical models with the accuracy of physical approaches for large simulations and control purposes [8-12]. The main advantages of these physics-based approaches rely on the possibility to express macroscopic variables (Cell Voltage) as a function of microscopic parameters and physical properties of the systems components.

The Li-ion battery is modeled as a superposition of three solid porous media, namely the positive

electrode, the separator and the negative electrode, all wetted by the electrolyte liquid phase that ensures the transport of Li ions from one electrode to the other. The classical one dimensional representation of the Li-ion battery is illustrated in Figure 1.
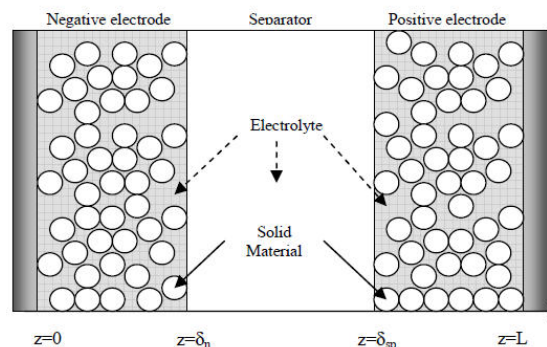

Figure 1: Schematic of the 1D-representation (z-axis) of a Li-ion battery cell.

2.1 Governing Equations

The governing equations of the electrochemical and thermal model are fully detailed in [13] and [14]. The model integrates the thermodynamic equilibrium potentials of the positive and negative electrodes (U_p and U_n), solid-phase mass balance within the spherical particles of the electrodes ($c_{s,p}(r)$ and $c_{s,n}(r)$), liquid-phase mass balance within the electrolyte along the z-axis ($c_e(z)$), and electrochemical kinetics at the electrodes/electrolyte interfaces. In this physics-based model, the cell voltage, V_{cell}, can be expressed as a function of cell design parameters, and physical-chemical properties of the system components (electrodes, separator, electrolyte...) as follows:

$$V_{cell}(t) = U_p\left(\frac{c_{s,p}^s}{c_{s,p,\max}}\right) - U_n\left(\frac{c_{s,n}^s}{c_{s,n,\max}}\right) + \ldots$$

$$\frac{2RT_{cell}}{F}\ln\left(\frac{\frac{-R_{s,p}}{6\varepsilon_{s,p}i_{0,p}A\delta_p}I + \sqrt{\left(\frac{R_{s,p}}{6\varepsilon_{s,p}i_{0,p}A\delta_p}I\right)^2 + 1}}{\frac{R_{s,n}}{6\varepsilon_{s,n}i_{0,n}A\delta_n}I + \sqrt{\left(\frac{R_{s,n}}{6\varepsilon_{s,n}i_{0,n}A\delta_n}I\right)^2 + 1}}\right) + \ldots$$

$$\left(1 - t_+\right)\frac{2RT_{cell}}{F}\ln\frac{c_e(L)}{c_e(0)} + \ldots$$

$$-R_{ohm}I - \left(R_{SLI,p} + R_{SLI,n}\right)I$$

(1)

Parameters signification can be found in the *"List of Symbols"* section. As described in [13-15], the

normalized surface Li ion concentration, $\theta = c_s^s / c_{s,max}$, can be used as an indicator to estimate the state-of-charge (SOC) of the battery. The definition of SOC differs from the one classically used in empirical equivalent electrical circuits modeling approaches as will be discussed below. The ionic conductivity of the electrolyte, κ, and the electronic conductivity of solid phases of the electrodes σ are considered. The ohmic resistance, R_{ohm}, is then expressed as the sum of ionic and electronic resistive contributions as follows:

$$R_{ohm} = \frac{1}{2A}\left(\delta_n \left(\frac{1}{\kappa_n^{eff}} + \frac{1}{\sigma_n^{eff}} \right) + 2\frac{\delta_{sep}}{\kappa_{sep}^{eff}} + \delta_p \left(\frac{1}{\kappa_p^{eff}} + \frac{1}{\sigma_p^{eff}} \right) \right) \quad (2)$$

Moreover, as thin resistive surface layers may grow on the spherical particle surface of the positive and negative electrodes as the battery system ages [13,16,17], resistive terms contributions ($R_{SLI,p}$ and $R_{SLI,n}$) are introduced in the cell voltage equation (Eq. 1):

$$R_{SLI,p} = \frac{\delta_{SLI}}{\kappa_{SLI} S_p} = \frac{\delta_{SLI} R_{s,p}}{\kappa_{SLI} 3\varepsilon_{s,p} A \delta_p} \quad (3)$$

$$R_{SLI,n} = R_{SEI} = \frac{\delta_{SEI}}{\kappa_{SEI} S_n} = \frac{\delta_{SEI} R_{s,n}}{\kappa_{SEI} 3\varepsilon_{s,n} A \delta_n} \quad (4)$$

As detailed in [13-14], an energy balance is used to compute the cell temperature, T_{cell}, and is described by the following equation:

$$\frac{d}{dt} T_{cell} = \frac{1}{M C_p}\left(\varphi_{gen} - \varphi_{tra} \right) \quad (5)$$

with the generated thermal flux

$$\varphi_{gen} = -\left(\left(V_{cell} - (U_p - U_n) \right) I + T_{cell} \frac{d(U_p - U_n)}{dT} I \right) \quad (5)$$

and the exchanged thermal flux

$$\varphi_{tra} = h_{conv} A_{cell} \left(T_{cell} - T_{amb} \right) \quad (6)$$

The electrochemical-thermal coupling is performed thanks to Arrhenius laws (Eq. 7) on both mass transport and kinetics parameters.

$$\Psi = \Psi_{ref} \exp\left(\frac{E_a(\Psi)}{R} \left(\frac{1}{T_{ref}} - \frac{1}{T_{cell}} \right) \right) \quad (7)$$

2.2   Model Parameters

As the battery cell internal parameters of the VL41M were not available through advanced intrusive characterization (cell dismantling), some assumptions were performed and most of the electrochemical and thermal parameters of the Li-ion battery model are taken from [4]. The calibration methodology is the same as performed in Prada et al. previous work [13]. Battery cell design parameters such as electrodes thicknesses and geometric areas are adjusted to obtain the rated capacity of 41 Ah according to equations 57 and 58 of Ref. 13. As will be discussed, the following results are parameters-dependent and highly rely on the quality of model parameterization.

2.3   Experimental Validation

The physics-based model was validated as illustrated in Figure 2 on a commercial Li(Ni$_x$Co$_y$Al$_z$)O$_2$/Graphite NCA/C 41 Ah cell as case study for this work. The validation procedure was performed on constant current discharge tests at C/3, 1C 2C and 150A. The data for the model validation were taken from the commercial data sheet [6]. The comparisons between experimental data and simulations at 20°C are presented in Figure 2.
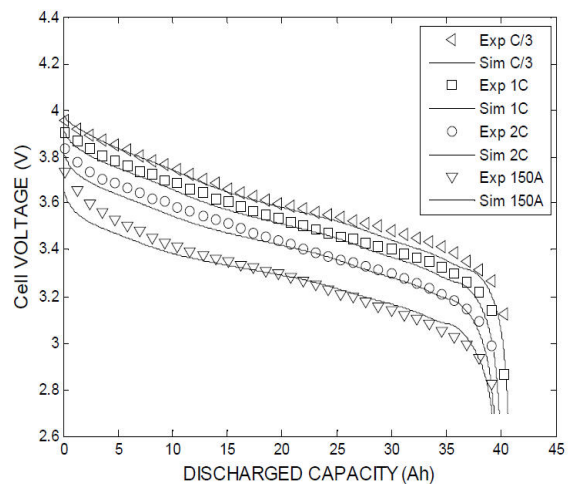

Figure 2: Comparison between experimental data (symbols) and model prediction (solid lines) for discharge curves at different current rates (C/3, 1C, 2C and 150 A) at 20°C

As observed, the agreement between experimental data (symbols) and model predictions (solid lines) is good. Errors on the cell voltage are lower than 50 mV over the full SOC range [0%-100%].

Moreover, the validation of the model provides interesting results even for high discharge rates (150 A namely 3.685C for the selected 41 Ah cell). Compared to classical equivalent electrical circuit modeling approaches where the SOC is computed by current intensity integration, the SOC of the battery in the physics-based approach is defined by the normalized spherical particle surface Li ions concentration, $\theta = c^s_s / c_{s,max}$. The concentration of inserted Li ions, c_s, is computed through a 1D-diffusion model (equation 3 in Ref 13) and thus provides dynamics that differ from a coulomb integration. As can be observed in Figure 2, the higher the discharge current intensity, the lower the discharged capacity extracted from the battery, due to mass-transport limitation phenomena.

3   Model-based Methodology for the Design of BMS laws

3.1   Methodology Flow chart

For the Li(Ni$_x$Co$_y$Al$_z$)O$_2$/Graphite (NCA/C) cell under study, the technical data sheet [6] provides the required constraints for maximal voltage, V_{max}, minimal voltage, V_{min}, and also maximal cell temperature, T_{max}.

Table1: Electrical and thermal constraints

	Voltage (V)	Temperature (°C)
Minimum	4.1	60
Maximum	2.7	-25

At any time, the BMS must indicate the allowable current limits for charge and discharge (CMI: Charge Maximal Intensity and DMI: Discharge Maximal Intensity) that the battery systems can safely supply/absorb at different temperatures (T) and states-of-charge (SOC) for a given pulse duration (t$_{pulse}$) without enforcing the voltage and thermal constraints, according to electric power absorbed by the vehicle operational usage. The CMI and DMI laws are generally specified by the battery manufacturer based on experimental tests campaigns. In the following subsection, the BMS laws specified by the battery manufacturer [1-2] are investigated for the Li(Ni$_x$Co$_y$Al$_z$)O$_2$/Graphite (NCA/C) Li-ion technology through a model-based methodology which allows the analysis of different physical phenomena that impact the system performance according to operating conditions.

The flow chart in Figure 3 presents a brief overview of the model-based methodology.
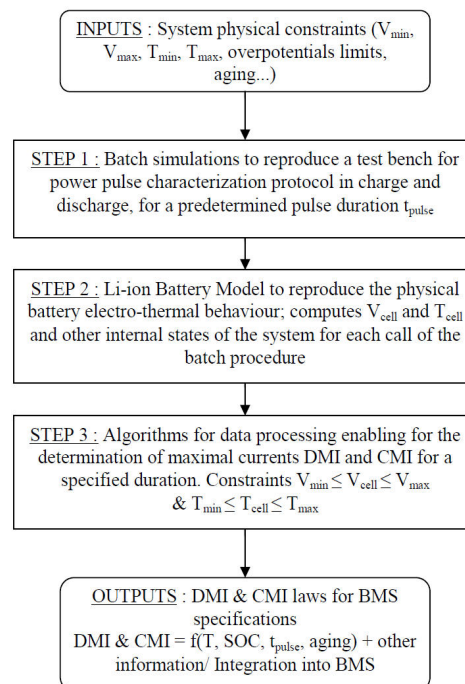

Figure 3: Block diagram of the proposed methodology

As shown in Figure 3, algorithms are designed to reproduce the test bench (Step 1), especially power pulse characterization in charge and discharge. The Li-ion battery model is used to reproduce the physical system electro-thermal behaviors (Step 2). During the batch simulations, the DMI and CMI are determined through the following constraints (Step 3), assuming pulses starting at t$_0$:

$$V_{min} \leq V_{cell}\left(t = t_0 + t_{pulse}\right) \leq V_{max} \qquad (8)$$

$$T_{min} \leq T_{cell}\left(t = t_0 + t_{pulse}\right) \leq T_{max} \qquad (9)$$

3.2   Preliminary Results and Analysis

As a first example, the model-based methodology for the design of BMS laws is used to determine the DMI at 30 s at different temperatures (from -25°C to 55°C) and SOC (from 5% to 95% SOC), while taking into account the abovementioned voltage and thermal constraints. Figures 4.a and 4.b represent two views of the simulated DMI at 30 s for the Li-ion cell under study. The DMI values correspond to the maximum discharge current the battery can provide during the pulse solicitation.
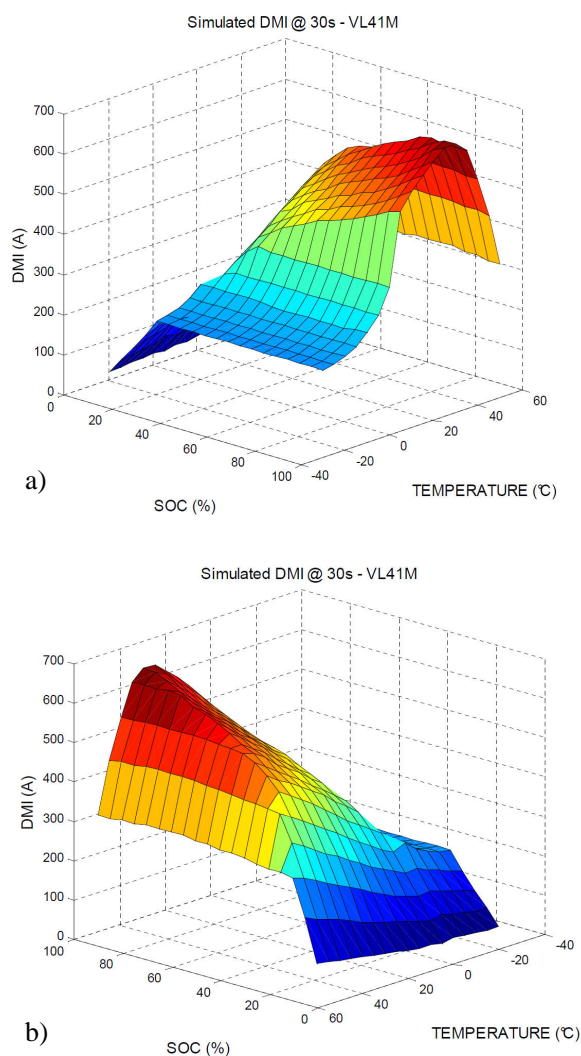
a)

b)

Figure 4: Simulated DMI at 30 s as a function of SOC
and temperature

Figures 4.a and 4.b show the impacts of temperature and SOC on the DMI at 30 s. At moderate temperatures (between 5°C and 35°C), the higher the SOC, the higher the DMI. Interestingly, an optimum is obtained for 95% SOC around 30°C.

Between 5°C and 35°C, the DMI is constrained by the minimal voltage, V_{min} and the DMI as a function of SOC has a classic shape as found for instance in reported data of the Freedom Car Test Manual [18]. For temperatures higher than 35°C, one can observe that the DMI decreases. At 55°C, the presence of a current limitation (current plateau) around 300A between 15% - 95% SOC (Figure 4b) is observed. This current limitation is due to the temperature constraint T_{max}. As the test temperature increases and gets closer to T_{max}, a lower current intensity is necessary to induce a temperature elevation. This

thermal-induced limitation explains why the DMI starts to decrease above 35°C. It is to note that the cell manufacturer specifies a value of 300 A for a 30s-discharge solicitation, which is very close to the current limit value given by our simulation at 55°C.

At low temperatures (T_{cell} = - 25°C for instance in Figure 4a), one can observe another current limitation between 25% and 95% SOC (current plateau). At this low temperature, the current plateau is due to liquid-phase mass transport limitations. Indeed, the Li ions concentration in the electrolyte phase, c_e, is almost zero which induces high mass transport overpotentials that limit the system power performances according to equation (1).

3.3 Comparison with battery manufacturers laws

In order to validate the proposed methodology, the BMS laws proposed by the cell manufacturers [1,6] were analysed and compared to our simulation results. Based on their patents, one can notice that the CMI and DMI specified by the manufacturer for the same chemistry (VL6P cell – NCA/C) but not the same typology (Power-type) are similar to the shapes observed at temperatures below 0°C and higher than 45°C i.e. where current-limited plateaus appear.
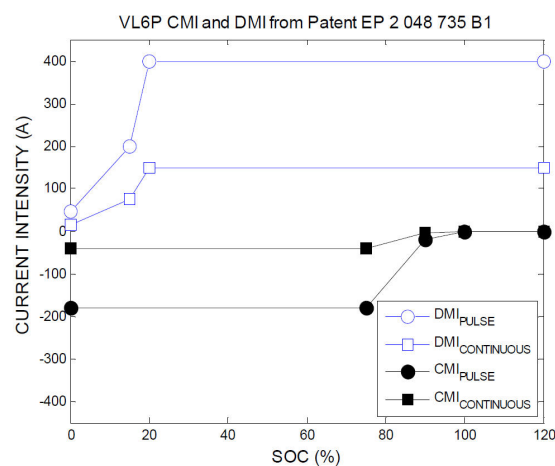

Figure 5: CMI and DMI designed by the manufacturer
for the VL6P cell.

Based on these observations, it seems probable that the manufacturer restricts the CMI and DMI to be conservative and to prevent too high charge or discharge currents in the range between 0°C and 55°C. Indeed, by restricting the computed DMI from Figure 4, one can determine the restricted specification. The following maps are computed by limiting the DMI by the values at 55°C.
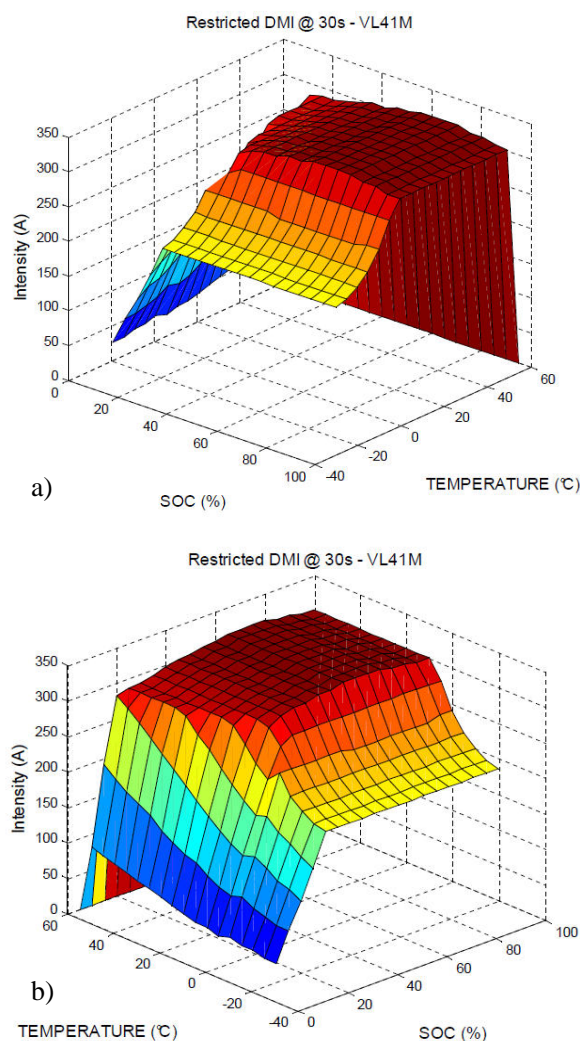
a)

b)

Figure 6: Restricted DMI at 30s as a function of SOC and temperature

Comparing Figure 5 and Figure 6, for a given temperature, the model-based methodology allows to retrieve similar shapes between simulated DMI and manufacturer BMS specifications. Practically, this means that higher power could be provided to/extracted from the battery system. Therefore, battery performances could be improved allowing for better use of the stored energy. However, careful attention has to be paid to high current solicitation that can generate stress-induced mechanical degradation phenomena at the electrodes level (particles cracking leading to accelerated aging). In the following section, the methodology is used to design CMI and DMI laws that could be introduced in a Battery Intensity Management Algorithm (BIMA) for (P)HEV and EV, for a battery pack composed of VL41M Li-ion cells.

# 4 Application of the Model-based Methodology for (P)HEV and EV

4.1 Background

In Ref [1], the four laws DMI_{PULSE}, $DMI_{CONTINUOUS}$, CMI_{PULSE} and $CMI_{CONTINUOUS}$, represented in Figure 5, are used in the BMS to manage the allowable current intensities that can be provided to/extracted from the battery system at any time as a function of SOC and temperature operating conditions.

As detailed in Ref [1] according to the battery application, Hybrid Electric Vehicle (HEV) for instance, high power pulses can be demanded to the battery, the values of which are higher than the maximum continuous current. Typically, according to the FreedomCar Test Manual [18], the duration of power pulses for HEV are around 10 to 30 s during charge or discharge phases. For power solicitations duration higher than 2 min, one can consider that the permanent (continuous) conditions are established. Due to mass-transport limitations, one can notice that the DMI and CMI values of continuous regime are always lower than those corresponding to power pulses solicitations.

In practical conditions, according to Ref [1], if a discharge power pulse at DMI_{PULSE} is demanded during $\Delta t > t_{pulse}$, a derating is applied to the current so that it converges to the $DMI_{CONTINUOUS}$ to ensure safe operation of the system.

4.2 CMI and DMI laws design

In this simulation case study, the power pulses duration is taken equal to 30 s for (P)HEV/BEV applications. The model-based methodology is then used to determine $DMI_{PULSE\ (30s)}$, $DMI_{CONTINUOUS}$, $CMI_{PULSE\ (30s)}$ and $CMI_{CONTINUOUS}$ for a fresh cell, i.e at the Beginning-Of-Life (BOL) state. The performance of the methodology strongly relies on the accuracy of the model prediction. In this context, the following results would have to be refined according to statistical studies on cell dispersion based on the model parameters and constraints, as well as with some experimental validation tests. This study will be performed for a future paper. Figure 7a/b represent the pulses and continuous intensity envelopes for charge and discharge phases that will be used in the battery intensity management algorithm (BIMA).
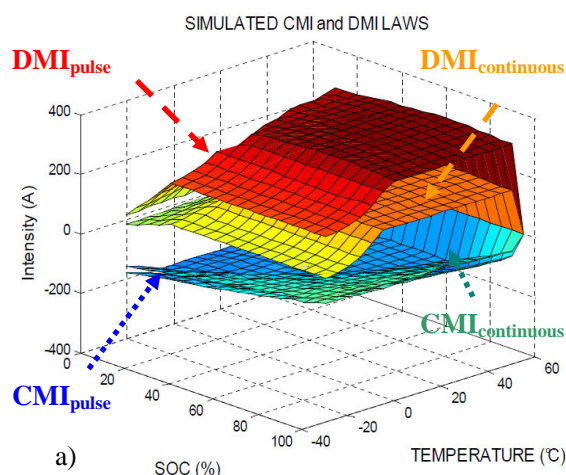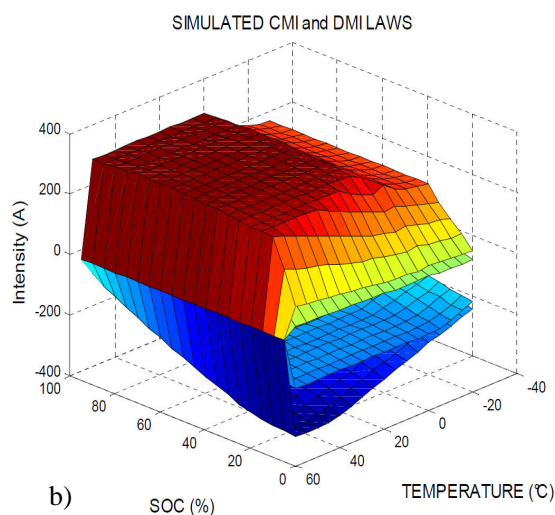
Figure 7: Simulated DMI and CMI for pulse and continuous operations as a function of SOC and temperature at BOL

4.3 Battery Intensity Management Algorithm (BIMA) Implementation and Validation

4.3.1 Software Architecture Overview

Instead of using the algorithm developed in Ref [1], an In-House Battery Intensity Management Algorithm (BIMA) has been designed and implemented on Matlab/Simulink Software. The software architecture is presented in Figure 8. As can be observed, the CMI and DMI laws determined for a given state-of-health (SOH) are implemented within look-up tables. The BIMA computes at each time the control current, $I_{control}$, without enforcing the DMI and CMI laws for pulse and continuous operation. If the demanded current, I_{demand}, does not induce enforcement of the security limitations of battery cell then the

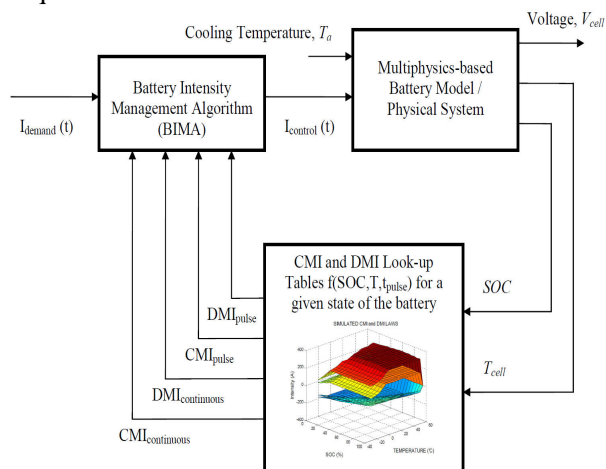demanded and the control current intensities are equal.

Figure 8: Representation of the Battery Intensity Management Algorithm implementation

The behavior is as follows. Once a change is detected in the sign of I_{demand}, a counter is reset and the 30 s-pulse CMI or DMI law is selected, depending on the current sign of I_{demand}. $I_{control}$ is computed accordingly. This counter is incremented at each execution of the algorithm. When it reaches 30 s, the maximum absolute intensity begins to decrease towards the corresponding value of the continuous law (this target is allowed to change from one execution to the other, according to SOC and temperature variations). This decrease can be managed through a first order filter, for instance. This can be easily extended to handle more than one duration for the pulse CMI and DMI laws. In the following subsection, the BIMA algorithm is numerically tested, analysed and validated on four case studies.

4.3.2 In-house Software validation tests

In order to validate the developed BIMA, simulations have been performed. The initial conditions of the four reported numerical tests are presented in Table 2.

Table 2: Electrical and thermal constraints

Simulation Case	Initial SOC (%)	Initial Temperature (°C)
N°1	70	+ 35
N°2	70	- 5
N°3	10	+ 35
N°4	100	+ 35

4.3.2.1   Case N°1 : Battery at intermediate SOC and T

Case N°1 represents a nominal operation of the battery system, namely at intermediate SOC (70%) and temperature (35°C). As shown in Figure 9, for this first simulation, even when not controlled, the cell voltage stays within the electrical voltage constraints V_{min} and V_{max}. However, it is observed (around 350 s and 475 s) that the BIMA limits the current when the solicitations exceed the pulse duration of 30 s.
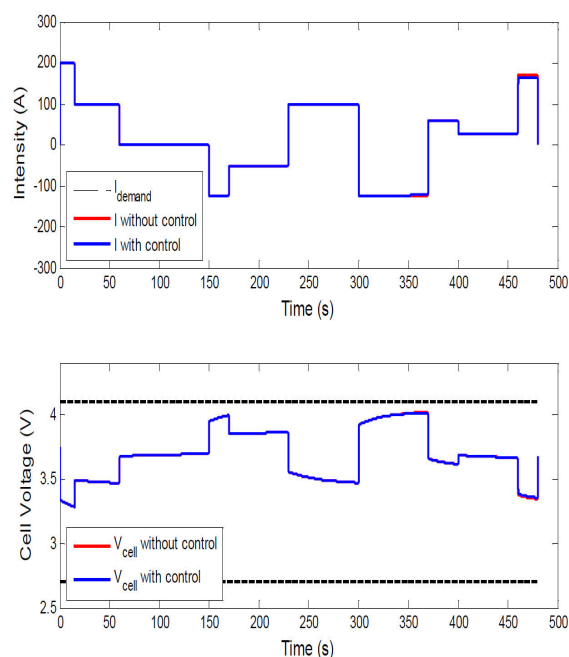

Figure 9: Evolution of Demanded, Uncontrolled and Controlled currents and the related Cell Voltages evolutions as a function of time for Case N°1

4.3.2.2   Case N°2: Cold Battery at intermediate SOC

In this second case, cold operation of the battery system is simulated (-5°C). As observed in Figure 10, the uncontrolled simulation (red line) stops prematurely around 165 s since the cell voltage reaches the upper cut-off voltage V_{max}. At cold temperatures, the battery performances are degraded as can be observed comparing cell voltage dynamics of cases N°1 and N°2. The controlled simulation allows for remaining within the voltage safety limits [V_{min}, V_{max}].
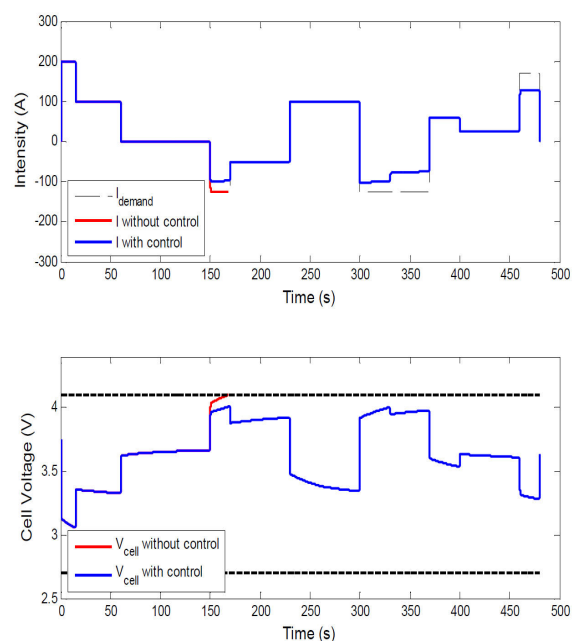

Figure 10: Evolution of Demanded, Uncontrolled and Controlled currents and the related Cell Voltages evolutions as a function of time for Case N°2

4.3.2.3   Case N°3: Undercharged Battery at intermediate T

The third case simulates a discharged battery at the beginning of service. This situation could represent the one experimented by an electric vehicle user who had forgotten to recharge the battery after the previous use. In this simulation, the initial SOC of the battery is 10%. The duty cycle is similar to case N°1. The duty cycle starts with a discharge phase of the battery. In the uncontrolled simulation, the battery cell voltage rapidly reaches the lower cut-off V_{min}, and the simulation stops prematurely after the first 10 s of the duty cycle profile. In the controlled simulation, the BIMA imposes a derating on the available discharge current intensity so that the battery does not reach its lower voltage limit and can provide energy to the powertrain even if the performance of the car would not be as high as in case N°1 for instance.
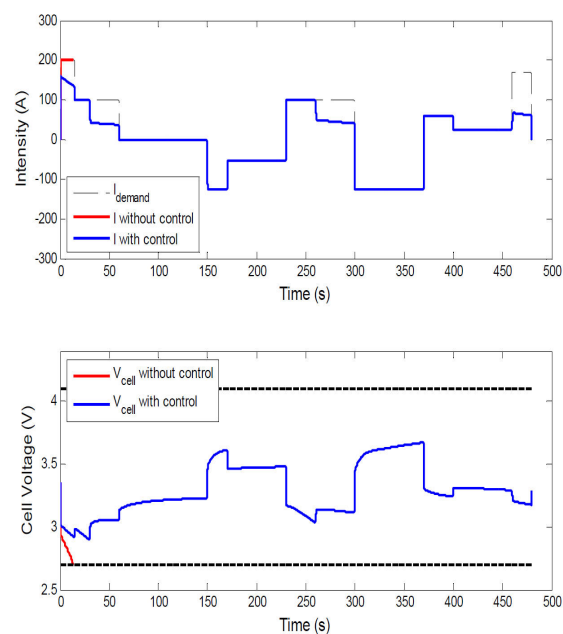
Figure 11: Evolution of Demanded, Uncontrolled and Controlled currents and the related Cell Voltages evolutions as a function of time for Case N°3

4.3.2.4   Case N°4: Overcharged Battery at intermediate T

The last case is similar to case N°3 but with a full charged battery. As represented in Figure 12, as the battery is fully charged, the discharge is allowed, leading to reduce the SOC of the battery.
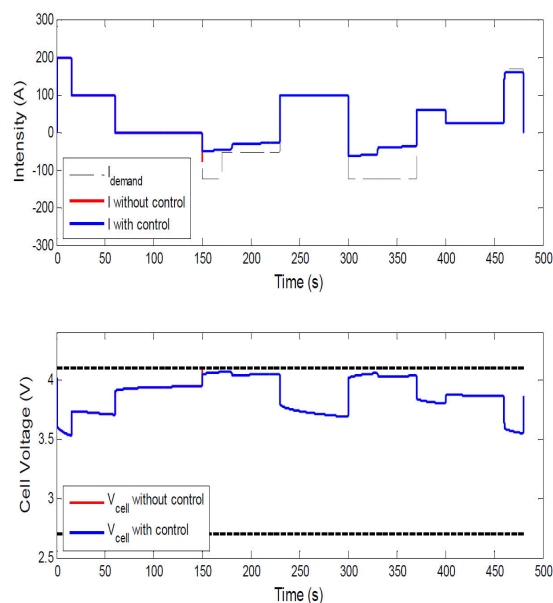

Figure 12: Evolution of Demanded, Uncontrolled and Controlled currents and the related Cell Voltages evolutions as a function of time for Case N°4

However, it is seen that, during the regenerative phases, the BIMA limits the charge current to prevent from overcharging the battery. In the uncontrolled simulation, the simulation stops around 150 s since the cell voltage reaches its upper limit.

5   Conclusions and Perspectives

In this paper, a multiphysics model-based methodology that allows for rapid and advanced BMS CMI and DMI laws development has been proposed and validated for Li-ion batteries. In a first step, the analysis of the DMI complex shapes as a function of SOC and temperature has been explained thanks to the model. The different physical limitations that constrain the battery performances have been identified such as thermal evolution at temperatures above 40°C, or liquid-phase diffusion at low temperatures, resulting in the presence of current plateaus that do not depend on the SOC. In a second step, these results have been compared to the battery manufacturers specifications and assumptions were discussed concerning the way the manufacturer restricts the CMI and DMI to be conservative. Based on these observations, CMI and DMI laws were designed for a commercial $Li(Ni_xCo_yAl_z)O_2$/Graphite (NCA/C) Li-ion technology, and implemented in an in-house Battery Intensity Management Algorithm (BIMA). Numerical validation of the proposed development has been performed to test different operating conditions that can be encountered in (P)HEV and EV applications. The performances of the methodology relies on the accuracy of the model prediction. In this context, the presented DMI and CMI results would have to be refined according to statistical studies on cell dispersion based on the model parameters and electrical constraints as well. This study will be performed for a future paper. Moreover, the methodology could be used to design CMI and DMI laws for aged cells so that the BMS would be conservative all along the battery lifetime.

List of Symbols

a_s active surface area (m^{-1})

A geometric area of the electrodes (m^2)

A_{cell} geometric area of the cell (m^2)

BMS Battery Management System

BOL Beginning-Of-Life state

c_e concentration of lithium in the electrolyte phase (mol m^{-3})

c_s concentration of reduced lithium in the solid phase (mol m^{-3})

c_s^s concentration of lithium at the solid-electrolyte interface (mol m^{-3})

C_p heat capacity (J kg^{-1} K^{-1})

E_a activation energy (J mol^{-1})

EOL End-Of-Life state

F Faraday constant (C mol^{-1})

h_{conv} thermal convective coefficient (W m^{-2} K^{-1})

i_0 exchange current density (A m^{-2})

I current intensity flowing through the system (A)

L length of the (-)/Separator/(+) assembly (m)

M cell mass (kg)

Ohm relative to the ohmic resistance

R ideal gas constant (8.314 J mol^{-1} K^{-1})

R_s radius of spherical particles (m)

SEI Solid Electrolyte Interphase

SLI Solid Layer Interphase

SOC State-Of-Charge (%)

SOH State-Of-Health (%)

t time (s)

t_{pulse} pulse duration (s)

t_+ Li ion transference number

T_{cell} cell temperature (K)

T_{min} Minimum cell temperature (K)

T_{max} Maximum cell temperature (K)

U thermodynamic equilibrium potential (V)

V_{cell} cell voltage (V)

V_{min} Minimum cell voltage (V)

V_{max} Maximum cell voltage (V)

x intercalated ratio of Li in the negative electrode

y intercalated ratio of Li in the positive electrode

z spatial coordinate in the 1D model (m)

Greek

α_{ox} charge transfer coefficient of anodic reaction

α_{red} charge transfer coefficient of the reduction reaction

δ lengths of electrodes and separator (m)

ε_e volume fraction of the electrolyte

ε_s volume fraction of the active material

ε_f volume fraction of the filler

θ normalized inserted Li ion concentration

η electrode overpotential (V)

κ ionic conductivity (S m^{-1})

φ thermal flux (W)

ϕ electric potential of electrolyte or solid phase (V)

σ solid phase conductivity (S m^{-1})

References

[1]   P. Desprez, G. Barrailh, S. Benjamin. *Charge Management Method for a battery.* Patent EP 2 048 735 B1, 2012

[2]   P. Baüerlein, F. Helmker. *Method for determining the amount of charge which can still be drawn from an energy storage battery, and an energy storage battery.* Patent US2004130297A

[3]   D. Di Domenico, Y. Creff, E. Prada, P. Pognant-Gros. *Estimation of Li-ion batteries available power for automotive applications.* Advanced Automotive Batteries Conference 2013

[4]   K. Smith, C-Y. Wang. *Power and thermal characterization of a lithium battery pack for hybrid-electric vehicles.* J. Power Sources 160 662-673, 2006

[5]   G. Plett. *Method for calculating power capability of battery packs using advanced cell model predictive techniques.* Patent US 7 969 120 B2, 2011

[6]   SAFT,   VL41M   Datasheet, www.saftbatteries.com

[7]   E. Prada, F. LeBerr, J-C Dabadie, R. Mingant, J. Bernard, V. Sauvant-Moynot. *Impedance-based Li-ion modeling for HEV and PHEV.* LMS Vehicle Conference, 2011

[8]   V. S. Kumar. *Reduced order Model for a Lithium ion cell with uniform reaction rate*

approximation.. J. Power Sources 222 426-441, 2013

[9] V. Boovaragavan, S. Harinipriya, V.R. Subramanian. *Towards real-time (milliseconds) parameter estimation of Lithium-ion batteries using reformulated physics-based model..* J. Power Sources 183 361-365, 2008

[10] X. Li, M. Xiao, S-Y. Choed. *Reduced order model (ROM) of a pouch type lithium polymer battery based on electrochemical thermal principles for real time applications.* Electrochimica Acta. 97 66-78, 2013

[11] J. Marcicki, M. Canova, A. T. Conlisk, G. Rizzoni. *Design and parametrization of a reduced-order electrochemical model of graphite/LiFePO$_4$ cells for SOC/SOH estimation.* J. Power Sources. 237 310-324, 2013

[12] J.L. Lee, A. Chemistruck, G.L Plett. *One-Dimensiona physics-based reduced-order model of Lithium-ion dynamics.* J. Power Sources. 220 430-448, 2013

[13] E. Prada, D. Di Domenico, Y. Creff, J. Bernard, V. Sauvant-Moynot, F. Huet. *Simplified electrochemical and thermal model of LiFePO$_4$-graphite Li-ion batteries for fast charge applications.* Journal of The Electrochemical Society 159 (9) A1508-A1519, 2012

[14] E. Prada, D. Di Domenico, Y. Creff, J. Bernard, V. Sauvant-Moynot, F. Huet. *A simplified electrochemical and thermal aging model of LiFePO$_4$-graphite Li-ion batteries: Power and Capacity Fade Simulations.* Journal of The Electrochemical Society 160 (4) A616-A628, 2013

[15] D. Di Domenico, A. Stefanopoulou, G. Fiengo. *Lithium-ion Battery State of Charge and Critical Surface Charge estimation using an electrochemical Model-based extended Kalman filter.* Journal of Dynamic Systems, Measurement and Control, 132, 061302, 2010

[16] D.P. Abraham, S. Kawauchi, D.W. Dees. *Modeling the impedance versus voltage characteristics of $LiNi_{0.8}Co_{0.15}Al_{0.05}O_2$.* Electrochimica Acta 53, 2121-2129, 2008

[17] H.J. Ploehn, P. Ramadass, R. E. White**,** *Solvent diffusion model of Lithium-ion battery cells.* Journal of The Electrochemical Society 151 (3) A456-A462, 2004

[18] FreedomCAR Battery Test Manual For Power-Assist Hybrid Electric Vehicles, http://avt.inel.gov/battery/pdf/freedomcar_manual_04_15_03.pdf

Authors

Dr Eric Prada graduated an engineering degree in 2006 and a Ph.D. in electrochemistry from the University Paris VI in 2012. He joined IFPEN in 2008, as a research engineer in the field of electrochemical energy storage systems (EESS) modeling. He is currently in charge of the battery modeling activities in the Electrochemistry and Materials Department with special focus on the battery degradation phenomena understanding and mathematical description. Since 2012, the developed EESS models are valuated through the commercial Electric Storage Library on the AMESim simulation software.
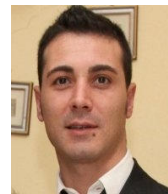
Dr Domenico Di Domenico obtained a PhD degree in Electrical Engineering and Computer Science at the "Università del Sannio" in 2008. During his PhD studies he was visiting student at the University of Michigan in Ann Arbor (USA). Presently he is a research engineer in automatic control at IFPEN in Lyon, France. His main research interest is the development and the application of innovative battery management strategies. His other research topics include urban traffic models and optimal power split for hybrid electric vehicles.

Dr Yann Creff graduated a Ph.D. in mathematics and control from the Ecole des Mines de Paris in 1992. He joined IFPEN in 2000, as a research engineer in the field of control science. He is now involved in various aspects of automotive control, and particularly in the design of algorithms for battery management systems.

Dr. Valérie Sauvant-Moynot is a Chemical Engineer with 14 years of experience at the French R& D IFP New Energy institute (IFPEN). Her various areas of work include development of pipelines anticorrosion and insulating materials, application of Electrochemical Impedance Spectroscopy, characterisation and modelling of batteries for automotive applications. Since 2007 she has been leading a competencies project on electrochemical storage systems. She

became head of IFPEN's "Electrochemical and materials" department of the Chemistry and Physico-chemistry Division in 2010